Lateral Soil Resistance and Reinforcement Effect around Pile Head
of Steel Pipe Pile with Wings

T. Kobayashi[1], Y. Miyamoto[2]

[1] *General Manager, Engineering Division, SANSEI Inc., e-mail: kobayashi@sansei-inc.co.jp*
[2] *Professor, Graduate School of Engineering Osaka University, e-mail: miyamoto@arch.eng.osaka-u.ac.jp*

Abstract

Recently, many different types of steel pipe piles with wings have been developed and put into practical use in mid- and low-rise buildings in Japan. These piles have flat or spiral-shaped steel wings welded to the pile tip or around the pile. Compared with cast-in-place concrete piles and bored piles, piles with wings have the advantages of reducing the amount of excavated soil and reducing environmental load. A steel pipe pile with wings is installed by applying a rotational torque to the pile shaft to screw the pile into the ground. The diameter of the wings is larger than that of the steel pile, resulting in loosening of the soil around the pile shaft. Consequently, the lateral subgrade reaction around pile is reduced. In the seismic design of steel pipe piles with wings, it is necessary to consider the reduced lateral soil resistance around the pile shaft. In this study, effect of the wings on lateral soil resistance was investigated by cyclic lateral loading tests in actual soil and three-dimensional finite element method (3D-FEM) analysis. The experiments were conducted for three cases: a pile with wings (W23) a pile without wings (ST), and a pile with wings reinforced with concrete around the pile head (IMP-W23). Here, IMP-W23 was examined to assess the effectiveness of improvement of the loosened soil around the pile head. At the test site, the soil affecting the pile lateral resistance is a soft clay layer. The load apparatus comprised a test pile, a reaction structure, and a hydraulic jack. Through these experiments, the lateral resistance at the pile head, bending moment distribution, and subgrade reaction were analyzed. Lateral loading tests were simulated using a 3D-FEM code, LS-DYNA. The analysis was performed by applying a forced lateral displacement at the pile head. The main results are as follows: (1) The lateral resistance of the pile with wings was smaller than that of the pile without wings. (2) The subgrade reaction of the pile with wings was smaller than that of the pile without wings, confirming the effect of the loosened soil around the pile head. (3) The lateral soil resistance of the concrete-reinforced around the pile head was improved in the wings passage region to a depth of 200 mm, becoming almost the same as that of the pile without wings. (4) Simulation analysis using 3D-FEM reproduced well both the pile head load and the bending moment distributions from cyclic lateral loading tests of the three types of piles.

Keywords: Steel pipe pile with wings, In situ cyclic loading tests, Soil spring, Pile head reinforcement, 3D-FEM

1. Introduction

Recently in Japan, many different types of steel pipe piles with flat or spiral-shaped steel wings welded to the pile tip or around the pile (hereinafter, steel pipe piles with wings) have been developed and used in low- and medium-rise buildings [1, 2]. Compared with bored piles, the use of steel pipe piles with wings is one method for reducing excavated soil and otherwise reducing environmental load. Steel pipe piles with wings are installed by applying rotational torque to the pile shaft to penetrate the ground. As the wings have a larger maximum rotational diameter during installation than the outer diameter of the pile shaft, the projections from the pile loosen the surrounding ground and affect the ground resistance around the pile head.

Several previous studies have investigated the lateral resistance of steel pipe piles with wings. Mori et al. [3] studied the coefficient of lateral ground reaction force k_h for the ground surface by monotonic lateral load testing. Kuze et al. suggested that the wings weaken the soil structure as they pass through and demonstrated through cyclic lateral loading tests that k_h decreases with increasing wing diameter ratio [4, 5].

We also previously conducted in situ cyclic lateral loading tests focusing on the presence or absence of wings, wing diameter ratio, and changes due to aging, finding that the wings are the factor that most strongly affects the subgrade reaction properties [6, 7]. We have also successfully reproduced the experimental results in simulations by reducing the initial shear stress G_0 and maximum shear stress τ_{max} [8, 9]. However, given that reduced subgrade reaction would also reduce the seismic performance of the piles, it would be preferable for the wings not to loosen the ground. In this paper, we present experimental results and three-dimensional finite element method (3D-FEM) simulation results for the effect of wings on the lateral resistance of piles and the reinforcement effect on the ground around the piles.

2. In situ cyclic lateral loading tests

2.1 Test site

Tests were conducted in Omitama City, Ibaraki Prefecture, Japan. The N-value distribution and soil boring log for the ground at the test site are shown in Fig.1. From the surface down, the ground at the site consists of Andosol, weathered volcanic ash, and sand. The soil affecting the pile lateral resistance is a soft clay layer with a small N-value.
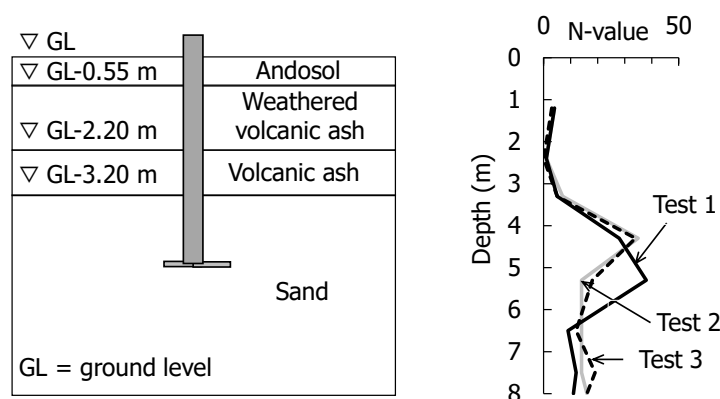

Fig. 1 – Results of ground survey at the test site

2.2 Test piles

The three test cases are shown in Table 1. Here, W23 is a steel pipe pile with wings and ST is a steel pipe pile without wings. In the IMP-W23 case, the soil around the pile head of W23 is reinforced with concrete in a 800 mm × 800 mm square to a depth of 200 mm. Photos 1 and 2 show the shapes of the pile tips for ST and W23, Photo 3 shows pile construction for IMP-W23, and Photo 4 shows the reinforcement of soil with concrete around the pile head. The maximum rotational diameter of the wings was 760 mm. The test piles were 5 m long with an outer diameter (D_p) of 267.4 mm and were made using steel pipes with a thickness of 9.3 mm. All the piles had closed tips with strain gauges attached to the inner surfaces of the steel piping.

Table 1 – Test cases

Test number	Specimen	
	Full name	**Abbreviation**
1	Steel pipe pile without wings	ST
2	Steel pipe pile with wings (wing diameter ratio 2.3)	W23
3	W23 with improved pile head	IMP-W23

Photo 1 – Steel pipe pile without wings (ST)

Photo 2 – Steel pipe pile with wings (W23)
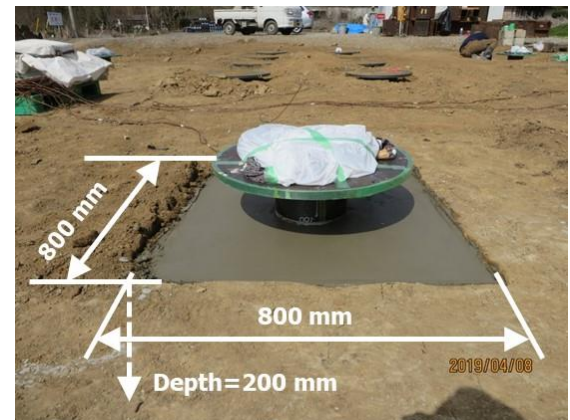

Photo 3 – Pile construction (IMP-W23)

Photo 4 – Concrete reinforcement of soil around the pile head (IMP-W23)

3

2.3 Methods for cyclic loading tests

The loading apparatus and measurement points are shown in Fig.2, and the test setup is shown in Photo 4. The loading apparatus comprised a test pile, a reaction structure, and a hydraulic jack. Main measurement items were pile strain, inclination angle of the pile head, lateral displacement at the loading height (ground level [GL]+400 mm), and the reference displacement, which was set at GL+100 mm. Cyclic lateral loading tests were controlled by the reference displacement, and pile head could freely rotate. The amplitude of the reference displacement was increased gradual from 1 mm to 100 mm in each cycle, with the loads applied twice in each direction. Subsequently, the reference displacement was increased up to 150 mm in the monotonic loading direction, completing the test.
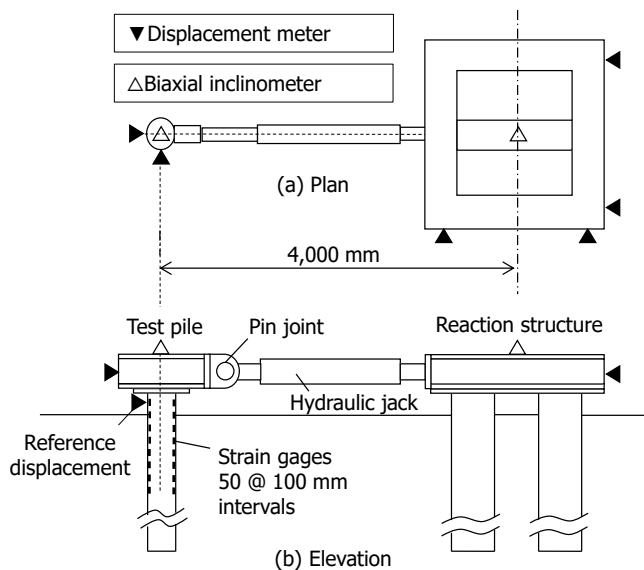

Fig. 2 – Experimental apparatus and sensor locations

Photo 4 – Experimental setup

3. Results of in situ cyclic lateral loading tests

3.1 Effect of presence or absence wings

In the test results, we focus on the reference displacement amplitude of 20 mm. The hysteresis curves of pile head load-reference displacement relationship are shown in Fig.3. The pile head load for W23 was around half that for ST. The distribution of pile bending moment at a displacement amplitude of 20 mm is shown in Fig.4. The maximum bending moment of W23 was smaller than that of ST and tended to occur at greater depths. Subgrade reaction–pile displacement relationships around the piles at each depth were calculated as explained previously [7-9]. The hysteresis curves at GL-0.5 m and GL-1.5 m are shown in Fig.5. The hysteresis curves for W23 at GL-0.5 m exhibited a clear S-shape with almost no subgrade reaction. Meanwhile, the hysteresis curves for W23 at GL-1.5 m did not exhibit an S-shape, although the subgrade reaction was smaller than that for ST. The secant stiffness ratios at several depths are shown in Fig.6. In the figure, the y-axis is the ratio of the secant stiffness of W23 to that of ST, and the x-axis is the pile displacement on a log scale. Note that the secant stiffness is calculated as explained previously [7-9]. The secant stiffness ratio increases with the displacement amplitude regardless of soil type, although there is a gap between these ratios for the Andosol layer and weathered volcanic ash layer. From the figure, the minimum secant stiffness ratios for the Andosol soil and weathered volcanic ash layer were approximately 0.1 and 0.2, respectively. The above results show that the presence of wings affected the lateral resistance and made the subgrade reaction smaller for W23 than for ST.
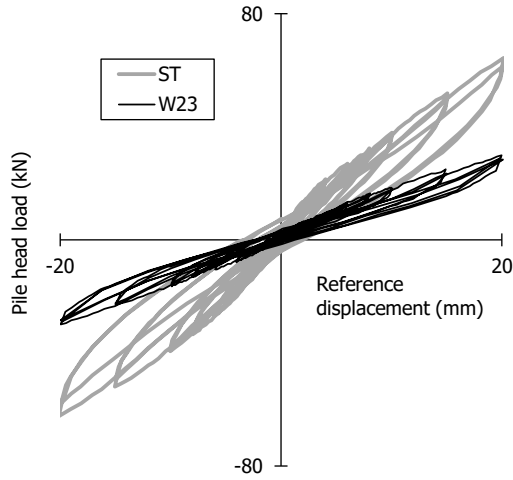
4

Fig. 3 – Pile head load vs. reference displacement
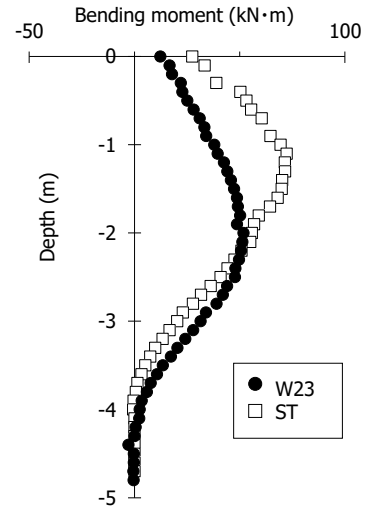(up to 20-mm displacement)

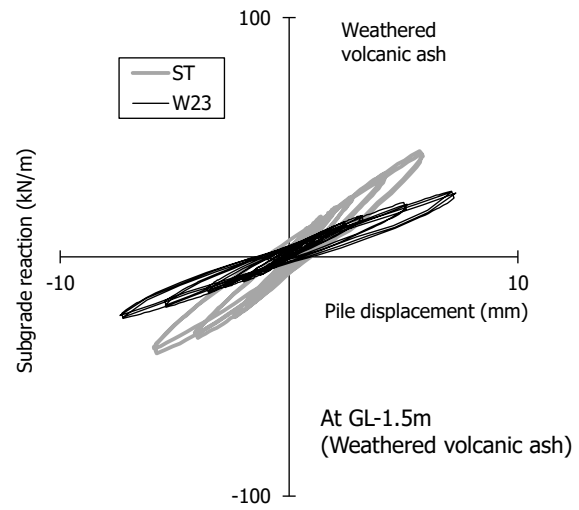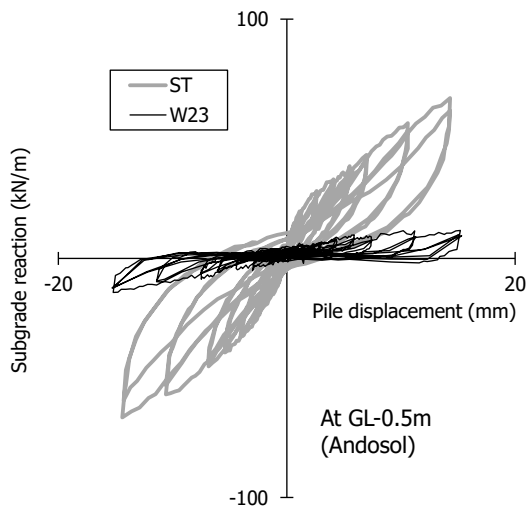Fig. 4 – Bending moment distribution
at 20-mm displacement

Fig. 5 – Comparison of subgrade reaction through the second 20-mm cycle: ST vs. W23

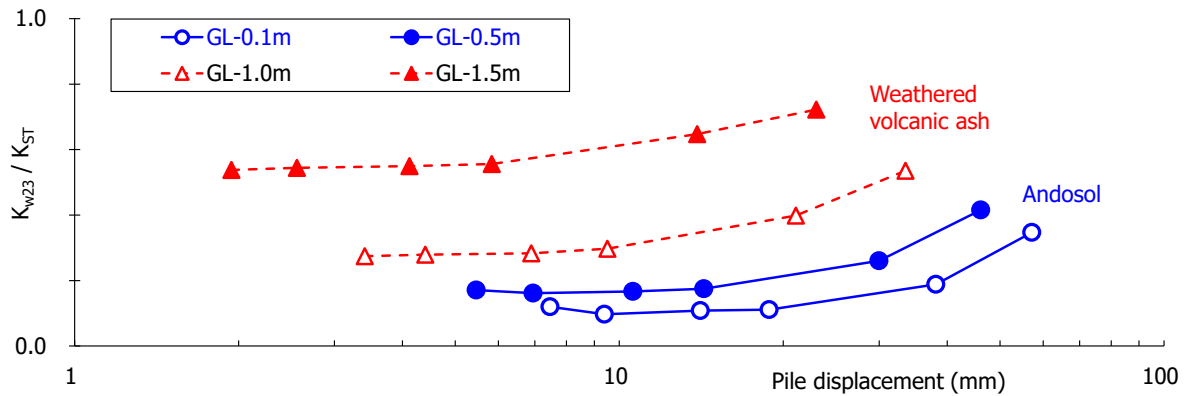Fig. 6 – Comparison of secant stiffness ratio of ST vs. W23

5

3.2 Effect of ground reinforcement around the pile head

The skeletal curve for the first cycle up to the reference displacement amplitude of 20 mm is shown in Fig.7. Here, the skeletal curve for IMP-W23 shows the same hysteretic properties as those of ST. The secant stiffnesses in Fig.8 were calculated for the first cycle at each reference displacement amplitude. In each test case, secant stiffness decreased with increasing the displacement amplitude, and the secant stiffness of IMP-W23 was equivalent to that of ST. Thus, ground reinforcement around the pile head appears to be an effective measure for increasing lateral resistance.
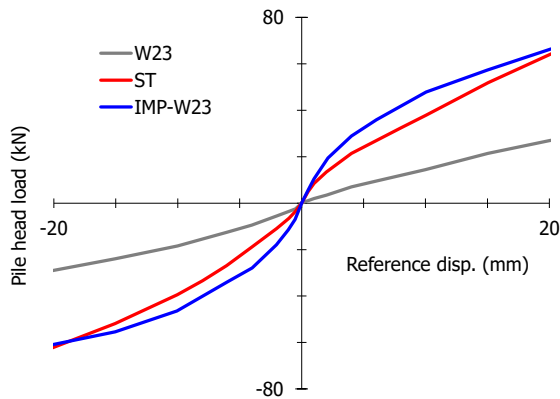

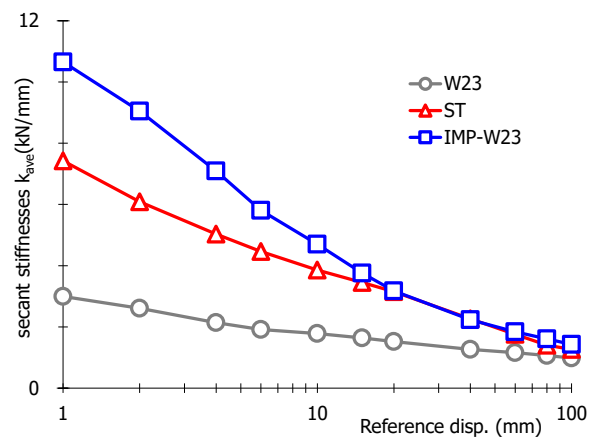Fig. 7 – Comparison of skeletal curves up to 20-mmdisplacement in the first cycle

Fig. 8 – Comparison of secant stiffness in the first cycle at each displacement amplitude

4. Simulation analysis

In situ cyclic lateral loading tests were simulated by 3D-FEM. For the analysis, a unidirectional monotonic load was applied to a freely rotating pile head to force lateral displacement. The analysis code LS-DYNA was used.

4.1 Nonlinear geotechnical properties

The physical properties of the site soil are shown in Table 2. The physical properties of the soil at the site were obtained by PS logging and triaxial compression tests for the soft clay layer. The material characteristic curve for the shear stress-strain behavior of the ground was approximated with a 10-line Hardin-Drnevich (HD) model. Fig.9 shows the material characteristic curve of the HD model. The Drucker-Prager yield coefficient was then applied to the shear stress at each segment point to account for dependence on confining pressure. The HD model is defined by Eq. (1) [10]:

$$G = \frac{G_0 \gamma}{1 + G_0 \gamma / \tau_{max}} \tag{1}$$

Here, G is shear rigidity, G_0 is initial shear rigidity, γ is shear strain, and τ_{max} is yield shear stress. Both G_0 and τ_{max} are calculated based on the soil type from the surface layer to GL-3.2 m and from GL-3.2 m downward.

6

Table 2 – Soil composition and material characteristics of ground at the test site

Layer	Depth	Ground classification	Wet density	Cohesion	Internal friction angle	Poisson's ratio	Initial shear rigidity	Max. shear stress	Reduct. coeff. of Dw region
			ρ	c	φ	υ	G_0	τ_{max}	region
	m		t/m³	N/mm²	deg.		N/mm²	N/mm²	
1	-0.55	Andosol	1.28	0.029	1	0.29	12.2	0.019	0.1
2	-1.40	Weathered volcanic ash	1.34	0.035	1	0.33	15.5	0.018	0.2
3	-1.70					0.33	15.5	0.018	
4	-2.20					0.49	15.2	0.018	
5	-3.20	Volcanic ash	1.64	0.090	1	0.47	15.2	0.024	
6	-4.70	Sand	1.80	0.001	30	0.45	58.3	0.027	1.0
7	-5.70					0.47	35.3	0.038	
8	-7.80					0.49	35.3	0.054	

1) Andosol, weathered volcanic ash, and volcanic ash from the surface layer to GL-3.2 m

Triaxial compression tests were repeated for this section, taking the secant stiffness of reference strain $\gamma_{0.5}$ and $\gamma = 10^{-4}$ as G_0 and calculating τ_{max} using Eq. (2):

$$\tau_{max} = G_0 \gamma_{0.5} \tag{2}$$

2) Sand from GL-3.2 m and below

As triaxial compression tests were not repeated for this section, G_0 was calculated using Eq. (3) and τ_{max} was calculated using Eq. (4), according to the Mohr-Coulomb failure criterion.

$$G_0 = \rho V_s^2 \tag{3}$$

$$\tau_{max} = \frac{\sigma_v + \sigma_h}{2} \sin \varphi + c \cos \varphi \tag{4}$$

Here, ρ is density, V_s is the S-wave velocity from P-S logging, σ_v is the normal stress at the reference depth, σ_h is the lateral stress at the reference depth, and φ is the angle of shearing resistance.

As the steel pipe pile with wings loosened the soil within the range of the maximum rotational diameter of the wing, reducing the lateral resistance of the ground around the pile head, G_0 and τ_{max} of the elements in this range were also reduced. The lower limits for the secant stiffness ratios for each ground classification given in Fig.6 were used for the reduction coefficients. Fig.10 shows the reduction region and the reduction coefficients.
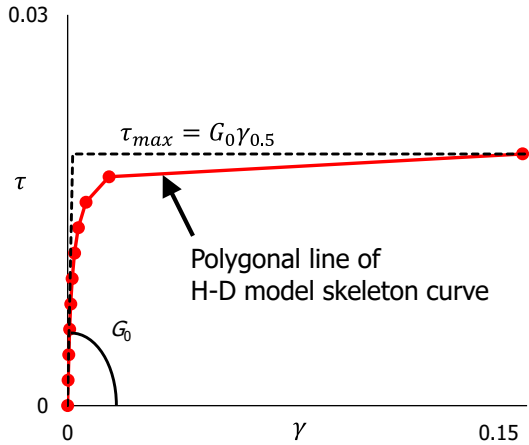
7

Fig. 9 –Material characteristic curve of the HD model

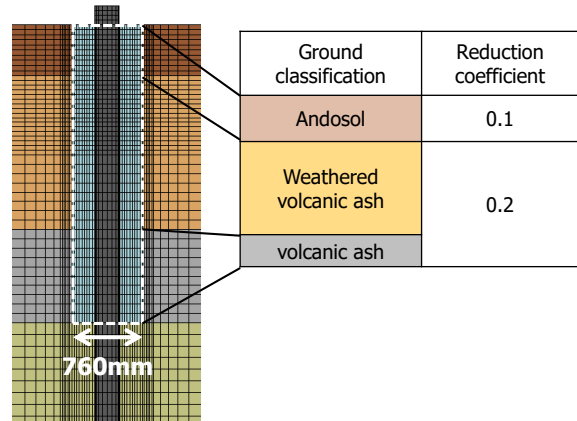Fig. 10 –Reduction region and reduction coefficients

4.2 Pile-ground modeling

The pile-ground analysis model used is shown in Fig.11. An elastoplastic body solid element was used for the ground. The ground was modeled 6 m in the loading direction (22 D_p), 2.6 m in the loading transverse direction (10 D_p), and 7.8 m in the depth direction, which is 3.0 m below the pile tip depth. The boundary conditions were a fixed base, vertical rollers on the sides, and elements divided into 8 segments in the depth direction. Contact conditions between pile and ground were also set to account for sliding, separation, and recontact. Thus, $\mu = \tan\varphi$ (where φ is the internal friction angle of each stratum) was used for the static and dynamic friction coefficients.

For the piles, D_p was divided into 16 segments using the shell element. An elastic modulus of $E_0 = 2.1 \times 10^5$ N/mm^2 and a yield strength of $\sigma_y = 315$ N/mm^2 (nominal value) were used for the strength properties of the pile material. The material properties were treated as a bilinear, reducing stiffness to $1/100 E_0$ when yield strength σ_y is exceeded.
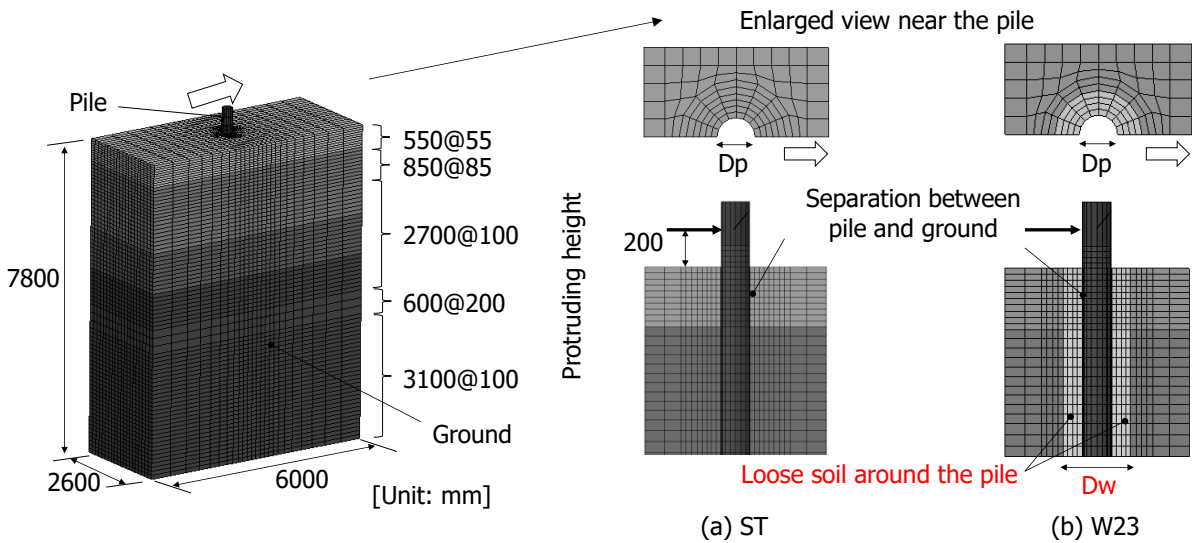
※ Boundary conditions of the FEM model were a fixed base with vertical rollers on the sides

Fig. 11 – Analysis model of pile and ground

8

4.3 Region of ground reinforcement around the pile–ground modeling

A contact model between the region of ground reinforcement around the pile head and the ground is given in Fig.12. Allowing for separation and slippage between the side face of the pile head in the reinforced region and the ground surface, a frictional coefficient of μ = 0.5 was used. No such allowances for separation and slippage were made between the bottom face and the ground surface. The properties of the reinforcement material used were set to be linear with an elastic modulus of $E_0 = 2.05 \times 10^4$ N∕mm^2 and a Poisson's ratio of v = 0.3.

Side of ground improvement

Set peeling and sliding coefficient of friction μ=0.5

ground improvement

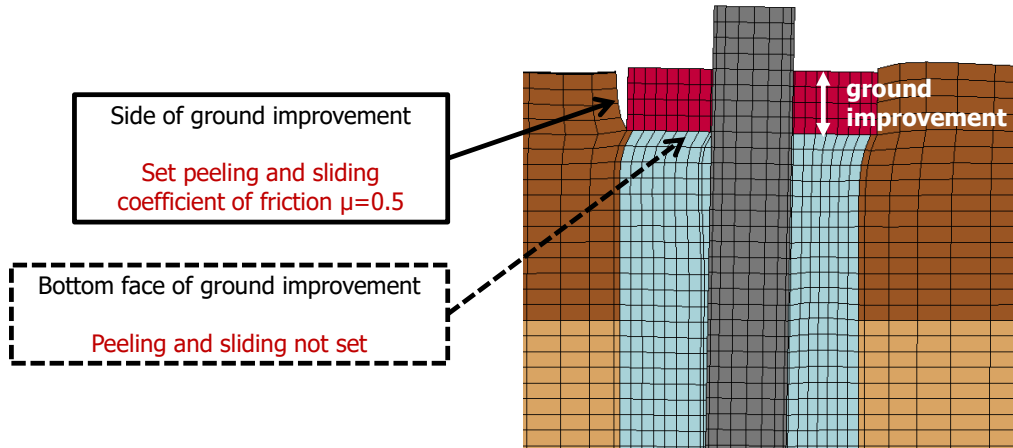Bottom face of ground improvement

Peeling and sliding not set

Fig. 12 – Contact condition between the pile and ground in the analysis model

4.4 Simulation results

The loading test and analysis results are shown in Fig.13 for comparison of the pile head load–reference displacement relationship. The ST test values corresponded well with the analysis values up to a ground pile displacement of 60 mm, at which point the pile is thought to begin undergoing plastic deformation. Meanwhile, all W23 analysis values exceeded the test values. The IMP-W23 test values were almost entirely consistent with the analysis values.

Bending moment distribution results at the reference displacement amplitude of 20 mm are shown in Fig.14. Analysis values for all cases corresponded well with the test values.
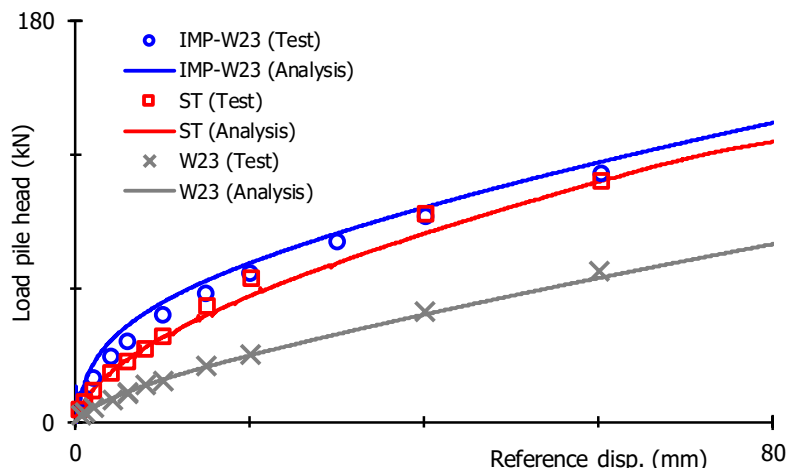
Fig. 13 – Comparison of test results and analysis results in all test case (pile head load vs. reference displacement)
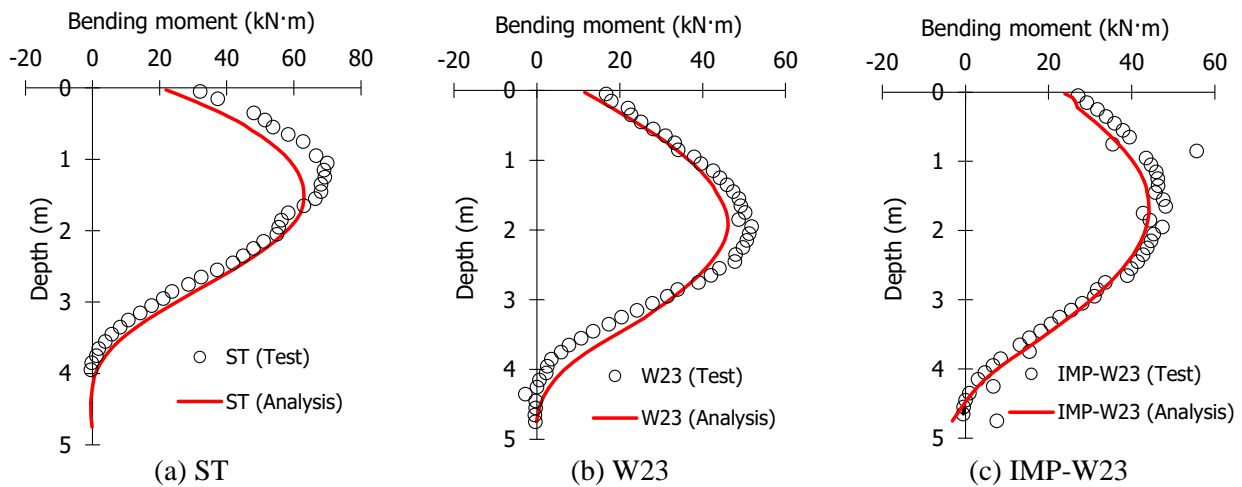
9

4e-0007

Fig. 14 – Comparison of test results and analysis results for bending moment distribution at 20-mm displacement

5. Conclusion

The main results of this study are as follows:

1) The lateral resistance of the pile with wings was smaller than that of the piles without wings.

2) The subgrade reaction of the pile with wings was smaller than that of the pile without wings, confirming the effect of the loosened soil around the pile head.

3) The lateral soil resistance of the concrete-reinforced pile head was improved in the wings passage region to a depth of 200 mm, becoming almost the same as that of the pile without wings.

4) Simulation analysis using 3D-FEM reproduced well both the pile head load and the bending moment distributions from cyclic lateral loading tests of the three types of piles.

Remaining issues for future research are to analyze and simulate the IMP-W23 test results for a larger amplitude range and to model an elastic bearing beam taking into account ground reinforcement around the pile.

Acknowledgements

Reference

[1] Tsuchiya T (2006): The trend of a screwed steel pile and the problems in the future [in Japanese], The Foundation Engineering & Equipment, Monthly, 34 (11), 2–6.

[2] Inoue N (2013): Recent trend of small-diameter rotating intrusive steel pipe pile construction method [in Japanese]. The Foundation Engineering & Equipment, Monthly, 41 (2), 36-39.

[3] Mori G, Hayashi M, Shinohara T (2000): Lateral loading behavior of screw steel pipe pile [in Japanese]. Japan National Conference on Geotechnical Engineering, 35 (727), 1755-1756.

[4] Kuze N, Suemasa N, Inoue N, Futaki M (2016): Property changes of soil around a rotary press-in pile with wings and lateral loading behavior of the pile. Journal of Structural and Construction Engineering (Transactions of AIJ), 81 (727), 1455-1465 (in Japanese).

[5] Kuze N, Suemasa N, Futaki M (2019): Influence of wings shape and cyclic loading on lateral loading behavior of a rotary press-in pile with wings in volcanic cohesive soil. Journal of Structural and Construction Engineering (Transactions of AIJ), 84 (758), 531-539 (in Japanese).

[6] Kashiwa H, Kobayashi T, Miyamoto Y (2018): Evaluation of lateral resistance of steel pile with wings in cyclic loading tests. AIJ Journal of Technology and Design, 24 (56), 99-104 (in Japanese).

[7] Kobayashi T, Nakano T, Kashiwa H, Miyamoto Y (2019): Study on lateral soil resistance around steel pipe pile with wings by static cyclic loading tests. Journal of Structural and Construction Engineering (Transactions of AIJ), 84 (759), 639-647 (in Japanese).

[8] Kobayashi T, Miyamoto Y (2018): Lateral resistance of steel pipe pile with wings by static cyclic loading tests. Dynamic Soil-Structure Interaction for Sustainable Infrastructures, GeoMEast, Cairo, Egypt, 40-52.

[9] Kobayashi T, Miyamoto Y (2019): Cyclic lateral loading test and simulation of lateral soil resistance for steel pipe pile with wings. Earthquake Geotechnical Engineering for Protection and Development of Environment and Constructions,7th International Conference on Earthquake Geotechnical Engineering, Rome, Italy, 3379-3387.

[10] Architectural Institute of Japan (2006): Seismic response analysis and design of buildings considering dynamic soil-structure interaction. Architectural Institute of Japan, Tokyo, Japan.